Microchimica Acta (2022) 189:414
https://doi.org/10.1007/s00604-022-05511-2

ORIGINAL PAPER

New carbon black-based conductive filaments for the additive manufacture of improved electrochemical sensors by fused deposition modeling

Jéssica Santos Stefano[1] · Luiz Ricardo Guterres e Silva[1,2] · Bruno Campos Janegitz[1]

Received: 18 July 2022 / Accepted: 23 September 2022 / Published online: 10 October 2022

Abstract
The development of a homemade carbon black composite filament with polylactic acid (CB-PLA) is reported. Optimized filaments containing 28.5% wt. of carbon black were obtained and employed in the 3D printing of improved electrochemical sensors by fused deposition modeling (FDM) technique. The fabricated filaments were used to construct a simple electrochemical system, which was explored for detecting catechol and hydroquinone in water samples and detecting hydrogen peroxide in milk. The determination of catechol and hydroquinone was successfully performed by differential pulse voltammetry, presenting LOD values of 0.02 and 0.22 μmol L^{-1}, respectively, and recovery values ranging from 91.1 to 112% in tap water. Furthermore, the modification of CB-PLA electrodes with Prussian blue allowed the non-enzymatic amperometric detection of hydrogen peroxide at 0.0 V (vs. carbon black reference electrode) in milk samples, with a linear range between 5.0 and 350.0 mol L^{-1} and low limit of detection (1.03 μmol L^{-1}). Thus, CB-PLA can be successfully applied as additively manufactured electrochemical sensors, and the easy filament manufacturing process allows for its exploration in a diversity of applications.

Keywords Composite filament fabrication · Carbon black · 3D-printed sensors · Prussian blue · Non-enzymatic detection · Differential pulse voltammetry

Introduction

3D printing technology is a form of additive manufacturing (AM) that has considerably revolutionized the methodological scenario of device prototyping of multifaceted structures with aerospace, electronics, food, medical, industrial, and academic applications [1, 2]. This technology goes beyond just manufacturing these materials, which is also strongly present in the scientific academic environment, especially in the area of analytical chemistry, through the production of additively manufactured electrochemical sensors [1, 3].

The most employed 3D printing technique in the manufacture of electrochemical sensors is fused deposition modeling (FDM), which consists of the deposition of melted filaments, creating three-dimensional objects layer by layer. This technique is the most affordable, and very advantageous for implementation in research laboratories for its low cost [1]. The recent use of conductive filaments in 3D printing allowed the manufacture of electrochemical sensors, which have been relevant in biosensing [4–6], food [7], environmental [8, 9], energy storage [10, 11], forensic [12], and biological analysis [6, 13], with distinguished characteristics, attributed to the use of AM, such as design versatility [12, 14]. For many years, the main conductive filaments used in the manufacture of 3D-printed electrochemical sensors were commercially obtained, and the most used ones were composed of graphene-PLA (G-PLA from Black magic®), and carbon black-PLA (CB-PLA from Proto-pasta®) [15, 16]. However, the composition of these filaments is poor regarding the amount of conductive material present. Therefore, the development of new composites for the manufacture of conductive filaments becomes a research area with great potential, which allows the production of specific filaments for the desired purpose.

To obtain electrodes with distinguished characteristics, Rocha et al. [17] performed the incorporation of $Ni(OH)_2$

✉ Bruno Campos Janegitz
brunocj@ufscar.br

[1] Department of Nature Sciences, Mathematics and Education, Federal University of São Carlos, Araras, São Paulo 13600-970, Brazil

[2] Department of Physics, Chemistry, and Mathematics, Federal University of São Carlos, Sorocaba, São Paulo 18052-780, Brazil

microparticles within a commercial G-PLA matrix. The developed electrodes were employed in the detection of glucose with low detection limits (2.4 μmol L^{-1}), and free from the interference of compounds typically found in biological samples. Innovatively, Foster et al. [18] proposed the production of a new conductive filament, composed of nanographite (25% wt.) within a PLA matrix. The produced filament originated from AM honeycomb structures, used in the simultaneous to detect lead (II) and cadmium (II) simultaneously. Our research group [13] proposed the production of new conductive filaments with high graphite loading (40% wt.), demonstrating for the first time, the development of ready-to-use additively manufactured electrodes that did not require a chemical or electrochemical pre-treatment step, just a simple surface polishing. The developed sensors were explored as a platform for the construction of an immunosensor for the detection of the spike protein of the SARS-CoV-2 virus and in the detection of the biomarkers uric acid and dopamine.

In this sense, the search for the easy and decentralized production of new conductive filaments, with the possibility to employ different compositions and materials has shown promising potential, enabling the AM of sensors with optimized and improved electrochemical characteristics, according to the needs. Carbonaceous compounds are very attractive options due to the wide variety of structures and sizes available, which can be chosen depending on their applicability. Also, the use of cheap carbon conductive materials is a great alternative. In this context, carbon black (CB) is a highly promising material, due to its electrical characteristics combined with high availability, easy acquisition, and low cost [19].

The conductive filament of CB is already commercially available, as previously discussed. Such filament is composed of a polylactide resin > 65%, polymer < 12.7%, and CB in a percentage mass < 21.4%, according to the manufacturer [20]. This filament was not obtained aiming the best conditions for specific applications, being constructed for generic applications. Therefore, the manufacture of CB filaments can be optimized, by employing adequate filament fabrication processes, capable to be performed in a laboratory, decentralizing the process, and allowing a variation in composition. In this way, the preparation of the CB-based filaments is attractive, by increasing the percentage of conductive material or changing other characteristics according to the desired purpose.

Therefore, the present work presents the lab-made manufacture of high-quality and optimized conductive CB-PLA filaments for the production of electrochemical sensors by AM. The electrodes obtained with CB-PLA filaments were evaluated for the voltammetric detection of catechol and hydroquinone in tap water samples, independently. Also, the proposed CB-PLA electrode was modified within Prussian blue (PB) particles, allowing the non-enzymatic amperometric detection of H_2O_2 in milk samples.

Experimental section

Reagents and materials

All solutions were prepared using ultrapure water, from a Milli Q® water purification system from Millipore (MA, USA), with resistivity higher than 18.0 MΩ cm. The reagents employed in this work were of analytical grade and used without further purification. Potassium chloride (≥ 99% w/w), ethanol (99.5% v/v), ferrocene methanol (97% w/w), and hydroquinone (≥ 99% w/w) from Sigma-Aldrich (St. Louis, USA); acetone (99.5% v/v), iron(III) chloride (97% w/w), and hydrochloric acid (37% v/v) from Synth (Diadema, Brazil); chloroform (99.8% v/v) from Qhemis (Indaiatuba, Brazil); sodium hydroxide (98% w/w), hydrogen peroxide (35% v/v), sodium phosphate dibasic (99% w/w), dimethylformamide (99.8% v/v), potassium ferricyanide (99% w/w), acetic acid (99.7% v/v), and phosphoric acid (85% v/v) from Dinamica (Indaiatuba, Brazil); potassium phosphate (98% w/w) from Cinetica (Jandira, Brazil); and pyro-catechol (99% w/w) and boric acid (99.5% w/w) from Vetec (Rio de Janeiro, Brazil).

Carbon black (VULCAN® XC-72R) from Cabot (São Paulo, Brazil) and pellets of polylactic acid (PLA) in natura from 3DLAB (Minas Gerais, Brazil) were employed for the obtention of the conductive filament. Commercial filaments based on carbon black and PLA (Proto-pasta®, obtained from Proto-Pasta, Vancouver, USA) were employed for comparison with the proposed carbon black filament. The electrochemical cells employed in this work were obtained using non-conductive PLA or ABS (acrylonitrile butadiene styrene) thermoplastic filaments, from Sethi3D (Campinas, Brazil).

Stock solutions of catechol and hydroquinone were freshly prepared in a 0.1 mol L^{-1} phosphate buffer solution pH 7.4, while hydrogen peroxide was prepared in a saline phosphate buffer solution (containing 0.1 mol L^{-1} KCl). The water samples were collected from two different taps in the laboratory, in the city of Araras, Brazil. Whole-fat milk samples were acquired in a local market in the same city. Both samples were simply diluted in supporting electrolytes (1:1 v/v) previous to the analysis.

Instrumentation and apparatus

All electrochemical measurements were performed using a potentiostat/galvanostat PGSTAT204 from Metrohm (Eco Chemie) controlled by NOVA 1.11 software, which also was used for acquisition of data and baseline correction of differential pulse voltammetric data, using the "moving average" algorithm, with window size set to 2. The electrochemical experiments were performed employing two types of electrochemical cells, both 3D printed using ABS or PLA filaments. For the initial studies, a

cylindrical cell, similar to the one presented by Cardoso et al. [21] was employed. This cell was used to evaluate the amount of carbon black on the obtained filaments, where the 3D printed working electrodes were shaped as a plate, and coupled at the base of the cylindric cell with the aid of screws and a rubber O-ring for avoiding leakage and delimit the geometric area (0.23 cm^2). A stainless-steel plate was used for the electrical contact, and a cover containing holes for coupling conventional reference ($Ag|AgCl|KCl_{(sat.)}$) and counter (Pt wire) electrodes also composed the cell, closing the circuit. Further experiments were performed employing a simpler cylindric cell, as illustrated in Fig. 1c. The cell was designed for working with three electrodes (reference, counter, and working electrodes), all manufactured by AM in a similar shape using the composite filament obtained. A circular structure at the tip of the electrodes is delimited as the electrode surface, using nail polish to cover the lateral and back parts of the electrode (where the redox processes are not interesting to occur), and has a diameter of 4 mm (geometric area of 0.13 cm^2), and a rectangle of 2.3 cm, where the potentiostat cable is connected. The cell was designed to work with 2 mL of solutions (complete coverage of the surface of the electrode), and the complete assembled cell is presented in Fig. 1c.

A Sethi3D S3 3D printer (Campinas, Brazil) was used for printing all the electrodes and electrochemical cells used in this work. The software Simplify 3D® was used for the control of the printer, and slicing of the image of the objects, previously obtained using the software Blender® (Fig. 1b).

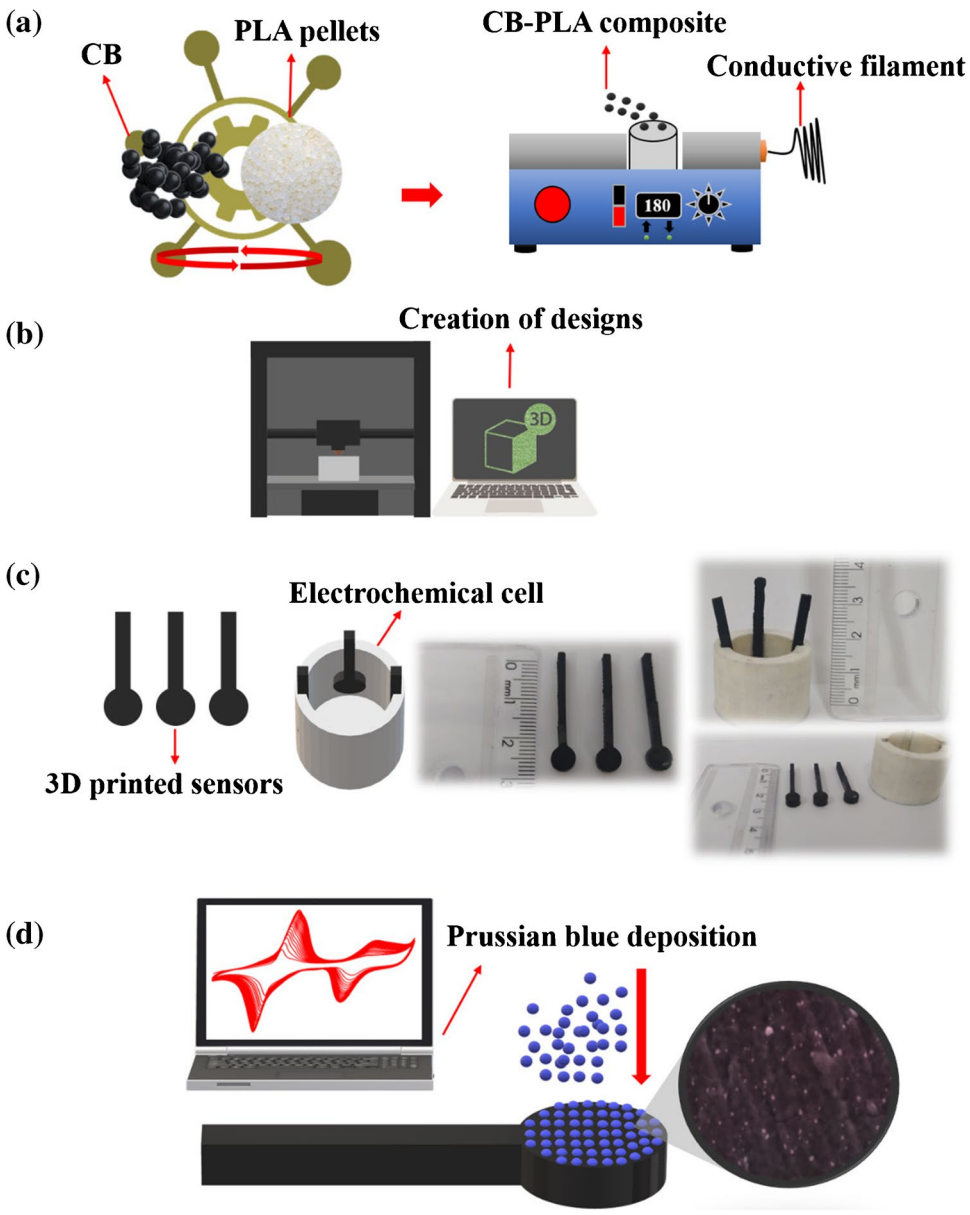

Fig. 1 Representative scheme of the experimental procedure: **a** Fabrication of CB-PLA conductive filament. **b** Obtention of electrochemical cell design and 3D printing preparation. **c** Image of the electrochemical cell and electrodes. **d** Scheme of PB electrochemical modification

The composite filaments were obtained using a Filmaq3D® extruder (Curitiba, Brazil), operated at a temperature of 180 °C (Fig. 1a).

Thermogravimetric analysis (TGA) was performed using a TGA 55 from TA INSTRUMENTS, in a gradual temperature increase of 10 °C per minute, varying from 25 to 1000 °C under oxidizing atmosphere. Raman data were obtained in a LabRam HR Evolution Spectrophotometer (HORIBA, Japan), using a 532 nm argon ion laser at 50 mW power over the range of 3500 to 70 cm^{-1}. Scanning electron microscopy (SEM) analyses were performed using a Thermo Fisher Scientific model Prisma E with ColorSEM Technology and integrated energy-dispersive X-ray spectroscopy (EDX), used for the acquirement of EDX spectra. For morphologic characterization of the carbon black particles, SEM measurements were performed in a CB film obtained for two different concentrated CB dispersions. The dispersions were prepared in a mixture of dimethylformamide (DMF) and water (1:1 v/v), and sonicated in an ultrasonic bath for 10 min. An aliquot of 100 µL was drop cast in the stub and left for drying overnight. Contact angle images were obtained with the aid of a smartphone camera, and a lab-made contact angle apparatus [22], by the drop-casting of deionized water on the electrode surface. After 10 s of the drop-casting the image was recorded, and the angle between the tangent drawn at the water droplet and the electrode surface was measured.

Fabrication of CB-PLA composite filament and electrodes

The composite of carbon black and PLA (CB-PLA) was obtained following the procedure reported previously by our research group [13], involving the production of a filament composed of graphite and PLA. Initially, carbon black powder was dispersed in 250 mL of a mixture of solvents (acetone and chloroform, 4:1 v/v) for 10 min under magnetic stirring (1500 rpm) in a reflux system. Vegetal oil obtained from a local market was used in the heating bath, and a digital thermometer was responsible to measure constantly the temperature of the system, kept constant at 70 °C. Next, pellets of PLA were added to the carbon black mixture, in which the amount of solids (carbon black and PLA) corresponds to a total of 30 g (8.55 g of CB and 21.45 g PLA), and left under reflux for 3 h. After this time, the recrystallization of the polymer, incorporated with carbon black particles, was performed by transferring the mixture to a recipient containing 800 mL ethanol and manually stirring with the aid of a glass rod. The composite obtained was then filtered, and washed with ethanol, to guarantee the recrystallization and consequent removal of the residues of acetone/chloroform solvents, and left to dry overnight in an oven at 50 °C.

After this process, the solid composite was partitioned into smaller pieces (< 2 cm), and extruded, giving rise to the homemade filaments. The filaments were employed for 3D printing of the electrodes by FDM, using a 0.4 mm hot end nozzle, with an extrusion temperature of 230 °C, and a heated bed temperature of 75 °C.

Surface pre-treatment

All the electrodes obtained by FDM 3D printing were polished using sandpaper (1200 grit) wetted with ultrapure water until the obtention of a smooth and homogeneous surface. The electrochemical activation was performed using a 0.5 mol L^{-1} NaOH solution, by the application of + 1.4 V during 200 s, followed by − 1.0 V during 200 s (vs. carbon black), as proposed by Richter et al. [8]. After activation, the electrodes were copiously rinsed with deionized water and coupled to the electrochemical cell for further measurements.

Preparation of the PB/CB-PLA electrodes

Electrochemical synthesis of PB film was performed following a procedure previously reported in the literature [23]. Twenty cyclic voltammograms were recorded at a scan rate of 50 mV s^{-1}, in a potential range from − 0.3 to + 1.3 V (vs. Ag|AgCl|$KCl_{(sat.)}$), in a solution containing 2.0 mmol L^{-1} $FeCl_3$, 2.0 mmol L^{-1} $K_3[Fe(CN)_6]$, 0.1 mol L^{-1} KCl, and 0.01 mol L^{-1} HCl. The synthesis was performed after polishing the electrode surface, and the electrochemical pretreatment described previously. After the film was electrodeposited (Fig. 1d), the electrode (PB/CB-PLA) was gently rinsed with deionized water, and employed for the detection of hydrogen peroxide.

Results and discussion

Characterization of the composites

For optimized exploration and evaluation of CB-PLA manufactured composites regarding their use as 3D-printed electrodes, filaments of varied compositions of carbon black were constructed (5.0 to 30.0% wt.). The percentage mass (CB loading) incorporated in the PLA was confirmed by TGA, and the effect of the temperature on each composite can be seen in Fig. 2a. Weight loss of CB-PLA occurred in two steps, which the first weight loss at around 350 °C is corresponding to PLA decomposition, and the complete loss is observed at around 600 °C due to the combustion of carbon black present in the composite [24]. It can be seen that the weight loss is depending on the amount of CB of each composite, indicating that the incorporation of

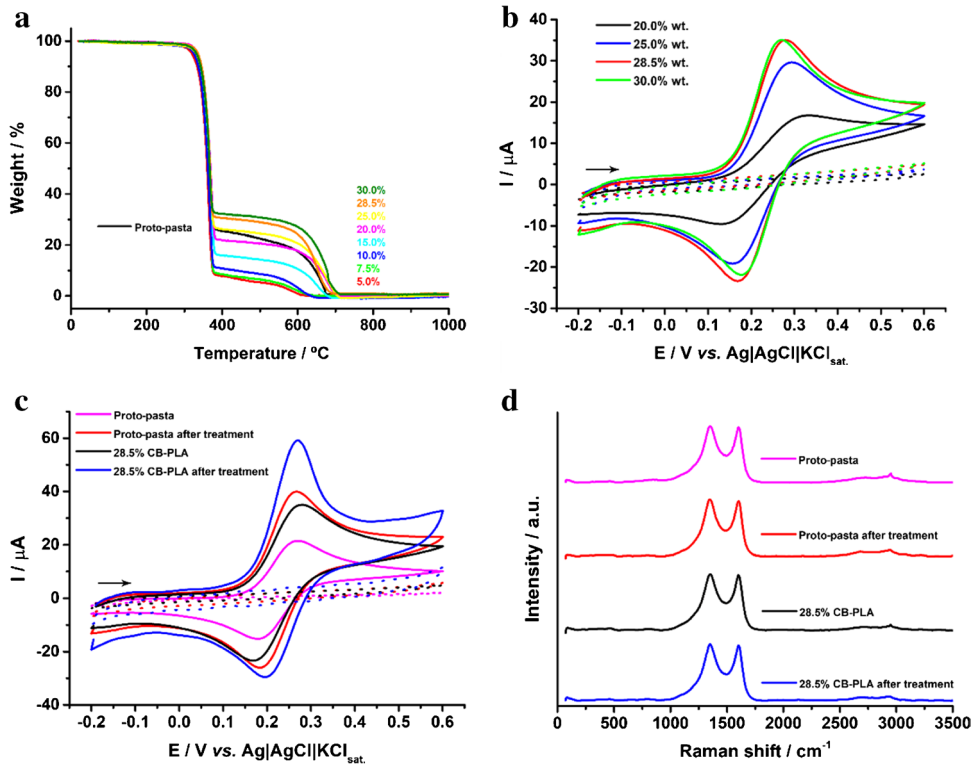

Fig. 2 **a** Thermogravimetric analysis for CB-PLA filaments of different carbon black loadings (5.0 to 30.0% wt.). **b** Cyclic voltammograms recorded for 1.0 mmol L^{-1} ferrocene methanol in 0.1 mol L^{-1} KCl, using CB-PLA 3D-printed electrodes obtained from the lab-made filaments with different carbon black loadings (from 20.0 to 30.0% wt.), and respective blank solutions (0.1 mol L^{-1} KCl—dotted lines). **c** Cyclic voltammograms recorded for 1.0 mmol L^{-1} ferrocene methanol in 0.1 mol L^{-1} KCl, using CB-PLA 3D printed electrodes obtained from the lab-made filaments containing 28.5% wt. carbon black, or commercial Proto-pasta filaments, both before and after electrochemical treatment. Dotted lines correspond to the blank solution. **d** Raman spectra for 3D-printed electrodes obtained with Proto-pasta and CB-PLA 28.5% wt. before and after electrochemical surface treatment

CB in different proportions was performed successfully. In addition, the TGA curve for the commercial Proto-pasta filament indicates CB loadings between 20.0 and 25.0%, agreeing with the real Proto-pasta composition (< 22% wt. of CB) [20, 25].

The electrochemical characterization of the composites was also performed. Cyclic voltammetric studies employing ferrocene methanol redox probe were conducted to evaluate the behavior of the different CB-loaded composites and the influence of electrochemical surface treatment. Composites with CB loadings lower than 20.0% wt. provided no electrochemical response, and those with CB loading composition higher than 30.0% wt. showed a challenging fabrication step. In the last case, due to the high amount of CB employed, the mixture of CB with PLA and the solvents employed in its solubilization provided a highly viscous solution, hindering the dissolution of PLA, and, consequently, the obtention of the composite. Thus, Fig. 2b shows the obtained voltammograms for CB-PLA 3D-printed electrodes containing 20.0, 25.0, 28.5, and 30.0% wt. CB. As can be seen, a significant improvement in the electrochemical response is observed with the increase in CB loading from 20.0 to 28.5% wt., providing a peak current two times higher and a more reversible process, with a ΔEp of 110 mV in contrast to the 202 mV from the composite containing 20.0% wt. The composite containing a higher percentage mass (30.0% wt.) provided no significant differences in the electrochemical behavior in comparison to 28.5%. Therefore, the optimized composite contained a CB loading of 28.5% wt., which was selected for subsequent studies.

The evaluation of the surface treatment effect in the obtained CB-PLA composite, and a comparison with the commercial CB filament (Proto-pasta), are presented in Fig. 2c. The cyclic voltammograms show that the surface activation using 0.5 mol L^{-1} NaOH solution promotes a significant increase in the electrochemical response, for both 3D-printed electrodes. Though a satisfactory response is observed for ferrocene methanol redox probe using the untreated electrodes, in agreement with the literature, for CB 3D-printed electrodes [26]. In this regard, the electrochemical surface treatment improved the response, providing current responses almost two times higher in both cases (1.7 times for CB-PLA

and 1.9 times for Proto-pasta). Also, better reversibility in the process is observed for both cases, with a considerable decrease in the peak-to-peak separation, especially for CB-PLA (decrease of 40 mV in ΔEp). This improvement can be attributed to the exposition of the CB particles, previously reported in the literature [8], which promotes the removal of the PLA from the electrode surface. This fact is because there is a partial saponification reaction (chemical activation), with subsequent potential pulses application (electrochemical activation). Experiments performed by electrochemical impedance spectroscopy (EIS) have shown that lower resistance to the charge transfer (*R*ct) value was observed after electrochemical activation of the surfaces (from 66.4 to 37.2 Ω for CB-PLA, and from 132.0 to 39.7 Ω for Proto-pasta), showing that the electron transfer is favored after the surface treatment. Figure S1 shows the Nyquist plots for CB-PLA and Proto-pasta3D-printed electrodes, before and after electrochemical treatment, in the presence of 1.0 mmol L^{-1} ferrocene methanol in 0.1 mol L^{-1} KCl.

The electrochemical response of CB-PLA 3D-printed electrodes obtained from the lab-made filaments was superior when compared to Proto-pasta. An increase of 48% in the peak current value is observed for CB-PLA when both electrodes are treated. The higher carbon black loading in the CB-PLA electrode can explain this behavior. CB-PLA has 7% more conductive material than Proto-pasta, which can facilitate the electron transfer process. EIS studies revealed a lower *R*ct value for CB-PLA, especially when both electrodes are untreated (66.4 Ω for CB-PLA and 132.0 Ω for Proto-pasta), which can indicate the reduced presence of polymer. In addition, a slightly lower *R*ct value was observed for treated CB-PLA (37. Ω) when compared to treated Proto-pasta (39.7 Ω) electrodes.

Raman measurements were performed for 3D-printed CB-PLA electrodes, obtained from the fabricated filament containing 28.5% wt. CB, and from commercial Proto-pasta filaments. In addition, the effect of surface treatment in Raman spectra was also evaluated for both electrodes. Fig. 2d shows the obtained spectra. The main peaks, typical of carbon black-based materials, are observed in all cases. The D band (1350 cm^{-1}) is related to the presence of defects in the structure and sp^3 hybridization, and the G band at 1600 cm^{-1} is associated with the presence of sp^2 carbon [27, 28]. The structural defects were calculated based on I_D/I_G ratio for each electrode. From I_D/I_G, values obtained (Proto-pasta: 1.12 and 1.13 before and after treatment, respectively; CB-PLA: 1.10 and 1.14 before and after treatment, respectively) can be inferred that the electrochemical treatment in both investigated electrodes did not insert structural defects, since no significant changes in the ratio intensity were observed. This result is in agreement with the literature, where 3D-printed electrodes were obtained using CB-based filaments either by the use of a 3D desktop printer or a 3D pen printer, and in both cases, no structural defects were inserted after electrochemical treatment [27]. Also, similar I_D/I_G values were obtained for both electrodes, thus, the number of structural defects at the electrodes obtained with the lab-made filament is the same as the observed for electrodes 3D-printed from commercial filaments. This result indicates that filaments fabricated in a laboratory, employing the procedure described in this work can replace the filaments obtained commercially.

Morphological characterization was also performed for the investigation of the 3D-printed electrode surfaces by the obtention of SEM images. Figure 3 presents the morphology of Proto-pasta 3D-printed electrode before (Fig. 3a) and after (Fig. 3b) the surface activation, in comparison to the lab-made CB-PLA, also before (Fig. 3c) and after (Fig. 3d) treatment. It can be seen, in both cases, that the surface treatment caused the appearance of more protrusions on both surfaces, evidencing the removal of the PLA excess from the electrodes. These protrusions can serve as active sites capable of improving the interaction of the species with the surface, which can corroborate the increase in current responses observed by cyclic voltammetric studies. The presence of CB can be noticed more clearly in treated CB-PLA, showing a similar structure to the observed for raw CB particles (Fig. S2). A brief discussion regarding SEM images from CB particles (Fig. S2) is presented in the supplementary material. In addition, both electrodes presented a comparable surface morphology, due to the similar composition. The PLA removal was confirmed by the contact angle measurements (inset figures). As can be seen, the AM structures presented a more hydrophilic behavior (contact angle values lower than 90°), which was expected due to the presence of oxygenated groups at the PLA matrix, reported previously in the literature [13]. In addition, the decrease in the contact angle after treatment, from 72° to 63° at Proto-pasta and from 60° to 55° at CB-PLA, indicate that the exposition of CB at both surfaces occurred. Since CB is an amorphous material, with a great number of sp^2 edge plans and containing oxygenated species over its structure [19], a hydrophilic character can be attributed to this material. Therefore, for materials containing a greater amount of CB, a decrease in the contact angle can be observed, confirming the exposition of this material after the surface treatment. The same fact can explain the reduced contact angle values from CB-PLA in comparison to Proto-pasta, which has 7% more polymer in its composition.

Furthermore, SEM analyses were also performed for CB-PLA 3D-printed electrodes obtained at different extrusion temperatures (200, 210, 220, and 230 °C). For its use as electrochemical sensors, the 3D-printed electrodes need to be uniform. The extrusion temperatures influence directly the presence of defects prevenient to the printing process [3], which were studied. Figure S3 shows the images obtained at each extrusion temperature before and after mechanical polishing, and the observations are discussed in the

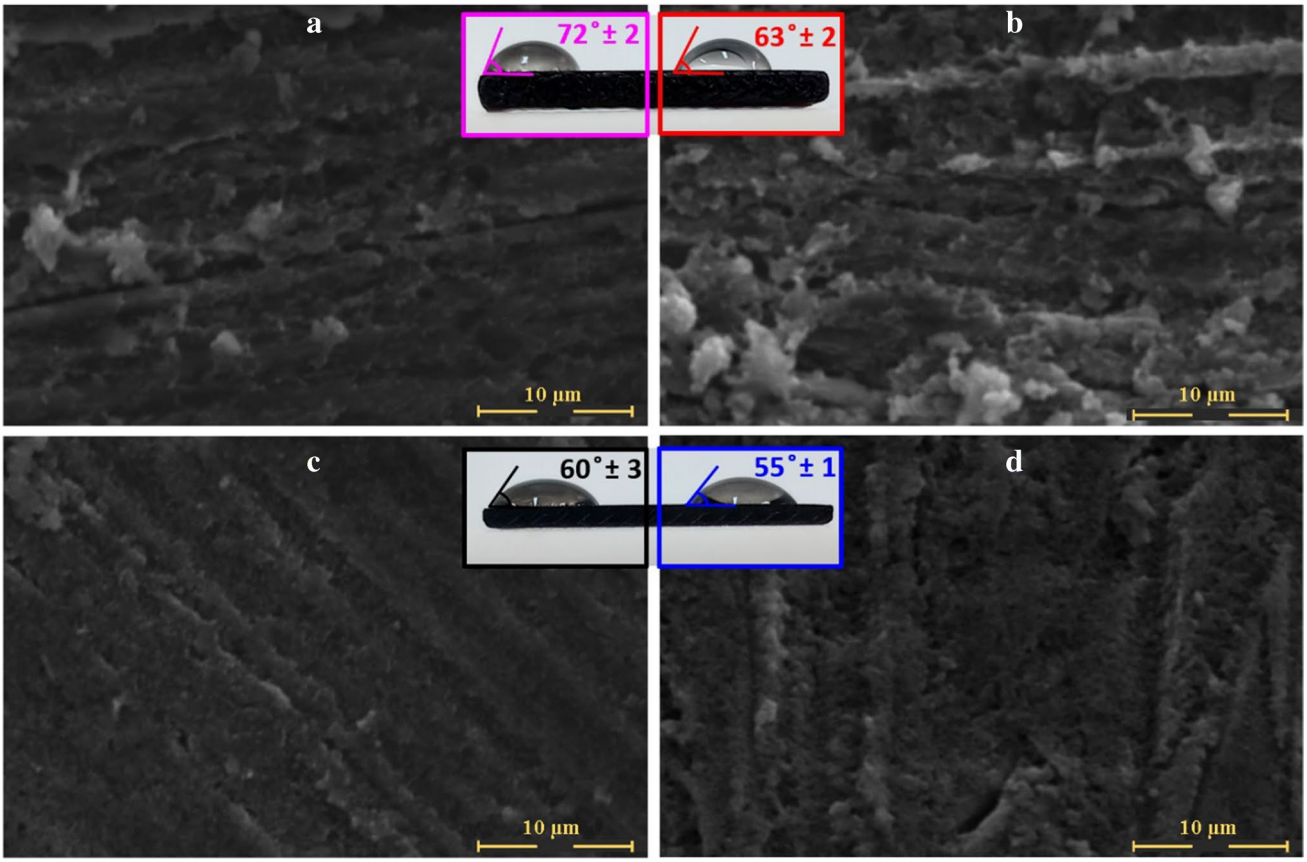

Fig. 3 SEM images for **a** Proto-pasta 3D-printed electrodes, **b** Proto-pasta 3D-printed electrodes after electrochemical surface treatment, **c** CB-PLA (28.5% wt. carbon black), and **d** CB-PLA (28.5% wt. carbon black) after electrochemical surface treatment, with amplification factors of 5000×. Inset: respective contact angle images

supplementary material, confirming the improved obtention of the sensors at a temperature of 230 °C.

The electroactive area of 3D-printed electrodes was evaluated by cyclic voltammetric measurements at different scan rates (10 to 100 mV s^{-1}) in the presence of 1.0 mmol L^{-1} ferrocene methanol, and estimated following the Randles-Ševčík equation for a quasi-reversible process [29]:

$$Ip = 2.63 \times 10^5 ACD^{1/2} n^{3/2} v^{1/2}$$

where I*p* is the peak current (A), *A* the electroactive area obtained (cm^2), *C* is the concentration of the redox probe (mol L^{-1}), and *D* is the diffusion coefficient of the redox probe (7.6×10^{-6} cm^2 s^{-1}) [30], *n* the number of electrons involved in the reaction, and *v* the scan rate (mV s^{-1}). Figure S4 shows the voltammograms obtained and the respective plots of anodic and cathodic peak currents as a function of the square root of the scan rate. A linear behavior was observed for both CB-PLA and Proto-pasta 3D-printed electrodes (even without surface treatment), showing that the mass transport process is diffusion controlled. The electroactive surface area values calculated for CB-PLA before and after surface treatment were 21.11 ± 0.01 mm^2 and 26.77 ± 0.13 mm^2, respectively, and for Proto-pasta, the electroactive area was estimated as 19.07 ± 0.13 mm^2 and 20.39 ± 0.30 mm^2 before and after surface treatment, respectively. As can be seen, the electrochemical treatment provided an increase in the electroactive area of the electrodes, confirming the exposition of CB after treatment. This increase was more accentuated at CB-PLA (increased 27%) 3D-printed electrodes than for Proto-pasta (an increase of 7%), showing a better exposition of CB at this surface. This fact is probably due to the higher amount of CB on this electrode surface. Lastly, for all studied surfaces, the values of electroactive surface area were higher than the geometrical surface area of the electrodes (12.57 mm^2) due to the electrodes' roughness, which is more pronounced at the treated electrodes. Table S1 shows the ratio between electroactive surface area and geometric area values ($A_{ratio} = A_{elect.}/A_{geom.}$), which provided values above 1.5, reinforcing the evidence of rough surfaces, as observed in SEM images. An improved discussion regarding the comparison between the electroactive area and the geometrical area is presented in the supplementary material.

Additionally, the heterogeneous electron transfer rate (HET) constant, k^0, was determined by EIS data from *R*ct values [31] for the studied surfaces, and the results show the faster electron transfer kinetics for CB-PLA in comparison to Proto-pasta, the results are discussed with more details in the supplementary material.

Finally, the batch-to-batch precision of the sensors was also evaluated. Figure S5 shows the cyclic voltammograms obtained with 4 different treated electrodes, 3D printed from CB-PLA filaments fabricated separately. The anodic peak currents provided an RSD of only 4.6%, showing that the filament fabrication process is adequate for the production of reproducible electrochemical sensors.

The superior performance of the electrodes fabricated using the manufactured CB-PLA filament was observed, with higher electroactive surface area, lower resistance to charge transfer, and consequent faster electron transfer rate. To evaluate the performance of CB-PLA as an electrochemical sensor, cyclic voltammetric studies were performed, using catechol (CA) and hydroquinone (HQ), followed by their detection using differential pulse voltammetry (DPV). Finally, the amperometric detection of hydrogen peroxide was also performed after surface modification of CB-PLA with PB.

Voltammetric detection of Catechol and Hydroquinone

Cyclic voltammograms were obtained using 1.0 mmol L^{-1} CA and HQ employing CB-PLA 3D-printed electrodes. The electrochemical behaviors of CA (Fig. 4a) and HQ (Fig. 4b) were explored to evaluate the surface treatment effect of CB-PLA at different compounds. The respective schematic representation of the redox mechanism for CA and HQ is also presented in Fig. 4c and d, respectively, showing the transfer of two protons and two electrons involved at CB-based electrodes, as reported in the literature [32, 33]. In both cases, the surface treatment provided a significant improvement in the electrochemical behavior of the molecules. An accentuated increase in the peak current (74%) is observed for CA, and the decrease in the Δ*E*p (from + 400 to + 160 mV) indicates the improvement in the reversibility of the process due to the exposed conductive CB at the electrode surface. An improvement in the electrochemical response of HQ was also observed, showing peak current values 53% higher than before the treatment, and a decrease in Δ*E*p from + 250 to + 167 mV.

Thus, the use of CB-PLA can be optimized by performing surface activation of the electrodes for the exposition of CB particles. For comparative purposes, the voltammograms from Fig. 4a and b were plotted in conjunction with other 3D-printed electrodes. Figure S6 shows the electrochemical behavior of CA and HQ in the proposed sensor in comparison to Proto-pasta, graphite-PLA (Gpt-PLA), and G-PLA 3D-printed electrodes, before (CA: Fig. S6-a, and HQ Fig. S6-c) and after (CA: Fig. S6-b, and HQ Fig. S6-d) surface treatment. As can be seen, for both CA and HQ, the proposed CB-PLA electrode (before and after electrochemical treatment) provided a superior response. The performance of lab-made filaments (CB-PLA and Gpt-PLA) is very satisfactory, even in absence of electrochemical surface

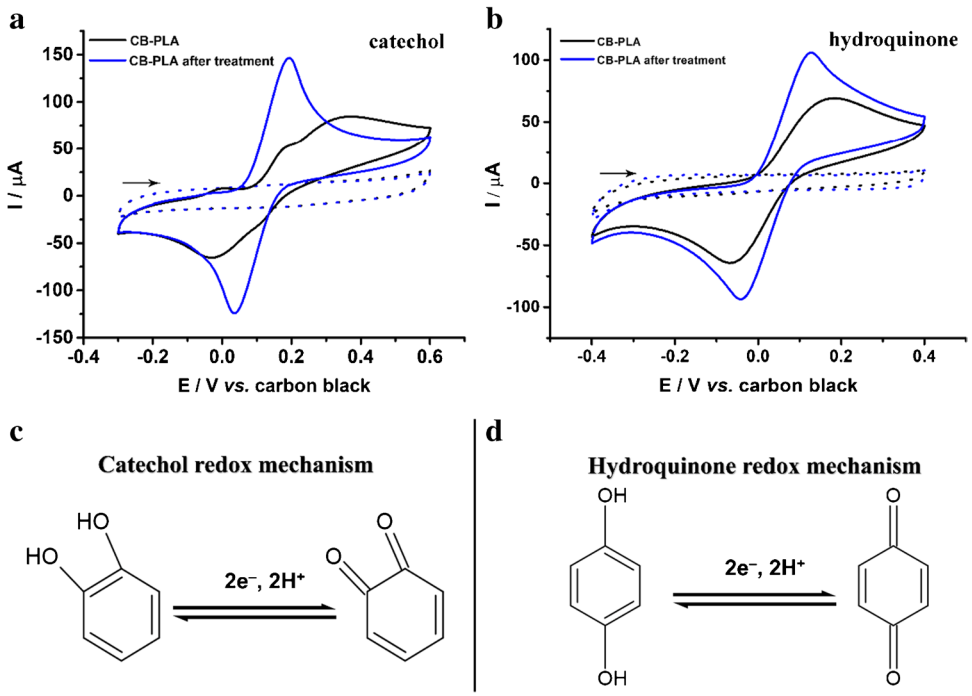

Fig. 4 Cyclic voltammograms recorded for 1.0 mmol L^{-1} **a** catechol; **b** hydroquinone using CB-PLA 3D-printed electrodes before (black line) and after (blue line) electrochemical surface treatment, and respective schematic representation of the redox mechanism for **c** catechol and **d** hydroquinone. Scan rate: 50 mV s^{-1}; Supporting electrolyte: 0.1 mol L^{-1} phosphate buffer solution (pH = 7.4); Dotted lines: respective blank solution

treatments, showing the importance of obtaining filaments with optimized composition. Furthermore, the reversibility of CB-PLA is improved in both cases compared to other electrodes. Current responses approximately twofold higher are obtained for CB-PLA in comparison to Proto-pasta, and approximately 3.5-fold in comparison to G-PLA for both CA and HQ. In comparison to lab-made Gpt-PLA, a peak current 1.6 times higher is obtained for CA at CB-PLA. For CA, CB-PLA current response is about 1.3 times higher, attesting to the superior performance of 3D-printed electrochemical sensors obtained with the proposed filament. Finally, it is noteworthy to mention that the electrochemical response of CA and HQ using untreated Gpt-PLA electrode is similar to the observed for dopamine, a similar molecule. These results are in agreement with those reported in a previous work in the literature [13], where no surface treatment was performed, showing the superior performance of lab-made filaments. To show the applicability of the proposed sensors, the voltammetric detection of CA was performed, exploring its oxidation process, as well as the voltammetric reduction of HQ, both in water samples.

The voltammetric oxidation of CA and reduction of HQ were performed independently, both employing treated CB-PLA electrodes. In this regard, the differential pulse voltammetric (DPV) technique was employed, using a 2 mL electrochemical cell. CA detection was performed employing DPV parameters adapted from the literature [34], fixing a step potential of 5 mV, modulation amplitude of 80 mV, modulation time of 20 s, and interval time of 0.5 s, and as supporting electrolyte, a 0.1 mol L^{-1} phosphate buffer solution (pH 7.4). The voltammograms were obtained in a range from − 0.05 to + 0.3 V (vs. carbon black). Figure 5a shows the voltammograms obtained for increasing concentrations of CA, and the respective analytical curve (Fig. 5b). A linear range from between 0.5 and 60.0 µmol L^{-1} was obtained for CA, following the equation: $I(\mu A) = 2.40 \times 10^{-8} + 1.84 \times 10^{-8}$ [CA], with a determination coefficient (R^2) of 0.993. The limits of detection (LOD) and quantification (LOQ) were calculated following IUPAC recommendations, where LOD = 3.3 σ /s and LOQ = 10 σ /s (σ is the standard deviation of the blank solution, and s is the sensitivity of the analytical curve). LOD and LOQ values of 0.02 µmol L^{-1} and 0.08 µmol L^{-1} were obtained, respectively. Finally, the analysis of CA in water samples was performed after fortification of two different samples at three levels of concentration each (5.00, 10.0, and 50.0 µmol L^{-1}) by using the DPV technique. Satisfactory recovery values (Table S2) were obtained for both samples, with values ranging from 99.0 ± 0.7 to 107 ± 2.5%.

The HQ detection was also performed following DPV parameters from the literature (step potential as – 4 mV, modulation amplitude of 50 mV, modulation time of 50 s, and an interval time of 0.5 s) [35]. The voltammograms were performed from + 0.4 to − 0.15 V (vs. carbon black)

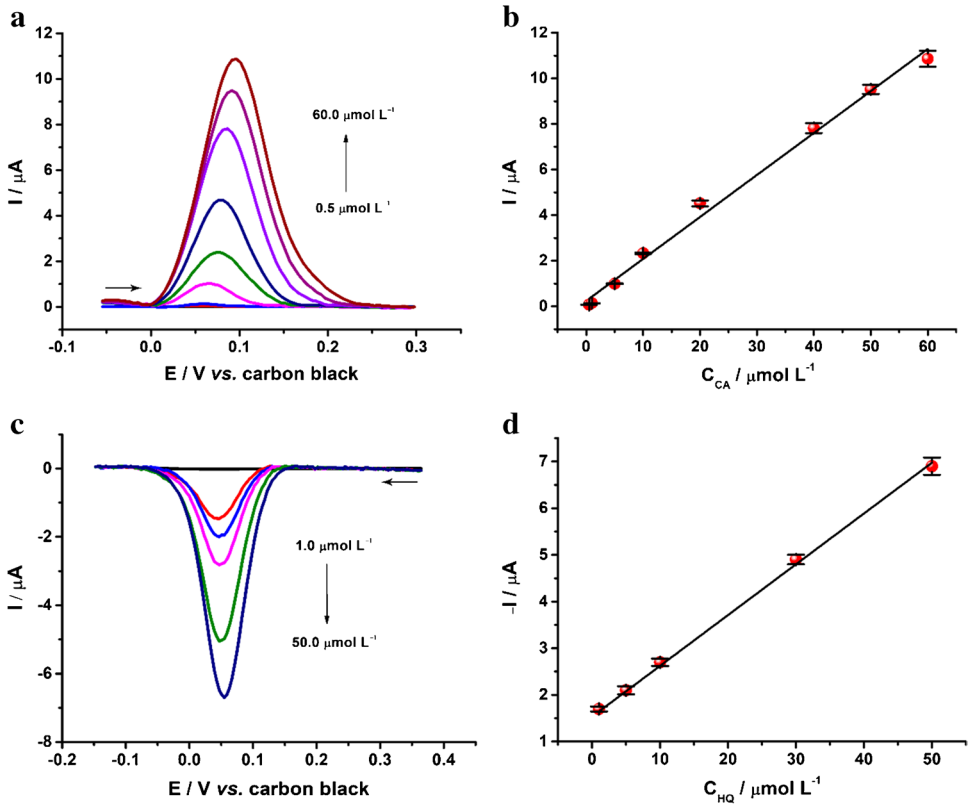

Fig. 5 DPV recordings for increasing concentrations of catechol (**a**) and hydroquinone (**c**), and respective analytical curves (**b**) and (**d**), obtained at the electrochemically treated CB-PLA 3D printed electrode; supporting electrolyte: 0.1 mol L^{-}.^{1} phosphate buffer solution (pH 7.4)

for increasing concentrations of HQ. Figure 5c and d shows the voltammograms and respective analytical curves for HQ at concentrations ranging from 1.0 to 50.0 μmol L^{-1}, respectively. A linear behavior was observed in the analytical curve of HQ, with the R^2 value of 0.999, following the equation: $-I(\mu A) = 1.53 \times 10^{-6} + 1.09 \times 10^{-7}$ [HQ]. Low LOD and LOQ values were obtained (0.22 μmol L^{-1} and 0.72 μmol L^{-1}, respectively) employing CB-PLA in the detection of HQ. For attesting the suitability, the analysis of HQ was also performed in water samples after spiking samples at three different concentrations (5.00, 10.0, and 30.0 μmol L^{-1}) by using the DPV technique. Recovery values ranging from 91.1 ± 6.5 to 112 ± 6.7% were obtained (Table S3), attesting to the suitability of the proposed method.

A comparison of the main performance characteristics obtained with the current CB-PLA 3D-printed sensor, with newly developed sensors for HQ and CA detection from the literature [6, 36–42] is presented in Table S4. According to the table, it is possible to observe that there are a variety of types of (bio)sensors used, such as glassy carbon electrodes, carb0n paste electrodes, and 3D-printed sensors, with the most distinct modifications. When comparing the analytical characteristics such as linear range and limit of detection, it is possible to observe that the sensors obtained in the present work showed excellent analytical responses when compared to the literature. In addition, it is worth mentioning that the use of 3D-printed sensors for the detection of the proposed analytes is still scarce in the literature, demonstrating the need to explore additive manufacturing for electroanalysis.

Amperometric detection of H_2O_2

Considering that PB is a remarkable material to be used as a modifier for its catalytic properties, allowing easy and non-enzymatic analysis of important biomarkers such as hydrogen peroxide and glucose [43–45], the 3D-printed electrode obtained in this work was also evaluated as a platform for surface modification, by the electrochemical deposition of PB. The modified electrode (PB/CB-PLA) was obtained following a simple procedure from the literature [23], by the electrochemical deposition (20 cyclic voltammograms) at the treated electrode surface. For the characterization of the modified electrode, SEM images were obtained before and after PB electrodeposition. Before the deposition of PB (Fig. 6a), a uniform and groovy surface are observed, with the absence of visible particles, only protrusions. After the electrodeposition (Fig. 6b), the presence of PB particles uniformly distributed is noted, indicating that the modification occurred successfully. EDX spectra obtained for PB/CB-PLA (Fig. S7) confirmed the presence of iron on the surface, and the semi-quantitative detection provided a considerable amount of iron (20.4 ± 1.7%), not present in the unmodified electrode.

Cyclic voltammograms were recorded at the PB/CB-PLA electrode for investigation of the PB film formation. The voltammograms were obtained in supporting electrolytes after the electrodeposition at both treated and untreated CB-PLA (Fig. 6c). In both cases, it is possible to observe the typical electrochemical behavior of PB, where four electrochemical processes are involved. The first process is occurring at

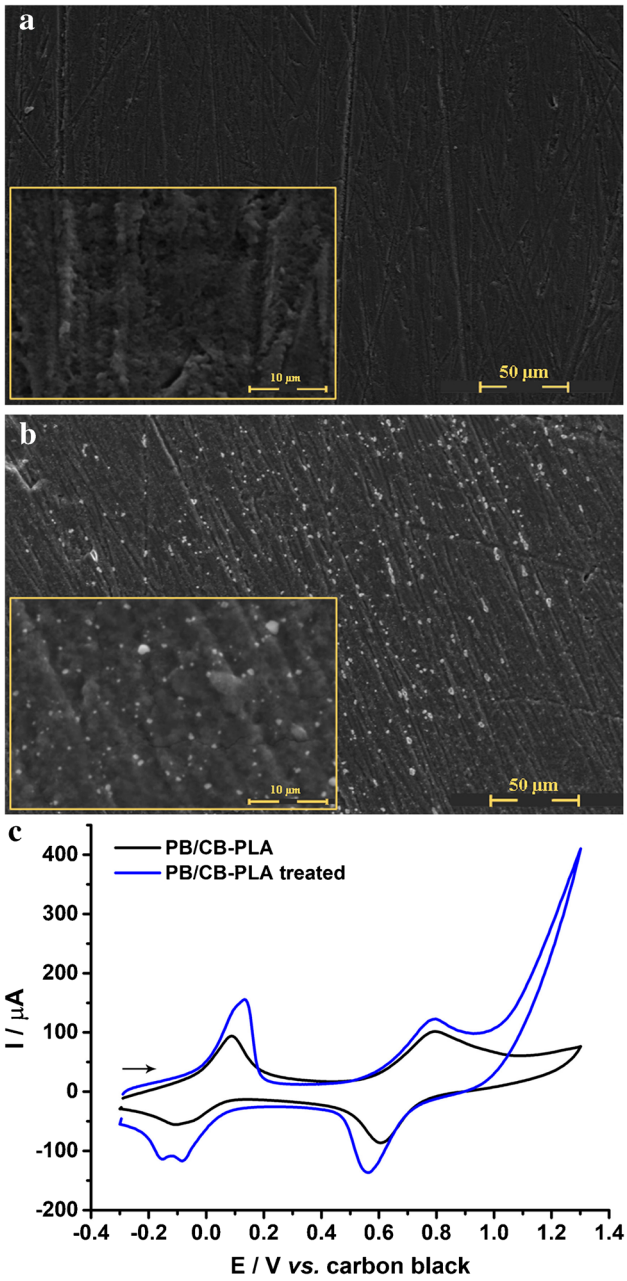

Fig. 6 SEM images of CB-PLA after electrochemical surface treatment before (**a**), and after Prussian blue electrodeposition—PB/CB-PLA (**b**), with amplification factors of 5000 x. **c** Cyclic voltammograms were obtained in 0.1 mol L^{-1} phosphate buffer solution (pH 7.4) containing 0.1 mol L^{-1} KCl at CB-PLA after modification with PB. Scan rate: 50 mV $s^{-.1}$

around + 0.1 V (vs. carbon black), and the corresponding reduction peak at around − 0.1 V (vs. carbon black), which are related to the Prussian blue/Prussian white pair, followed by the second oxidation process, at around + 0.8 V (vs. carbon black), with the respective reduction at + 0.6 V (vs. carbon black), referent to Berlin green/Prussian blue pair [46]. As can be seen, PB is formed on the CB-PLA surface even without surface treatment; however, an increase in the current peaks is observed after surface treatment, together with a slight reduction at the peak potentials. In addition, the electrochemical response of hydrogen peroxide on PB-modified electrodes is increased at the treated electrode. For evaluation of the surface treatment effect at hydrogen peroxide electrochemical response, the voltammetric behavior of hydrogen peroxide was evaluated at the CB-PLA electrode before and after surface treatment. For this, PB modification was performed at the treated and not treated CB-PLA surface, and the voltammograms of Fig. 7a show the effects of this treatment.

The dotted lines observed in the voltammograms correspond to the response of the supporting electrolyte, and the redox process observed at + 54 mV and – 130 mV corresponds to PB on the electrode surface. As can be seen, the electrochemical reduction of hydrogen peroxide (solid lines) occurs at PB/CB-PLA with or without surface treatment. The mechanism involved in the reduction of hydrogen peroxide on PB-modified surfaces is presented in Fig. S8, in which the hydrogen peroxide reduction by Prussian white occurs, involving the transfer of two electrons from the electrocatalyst to hydrogen peroxide, producing OH^- [47, 48]. When the treated electrode is employed, a slight increase of the reduction peak is observed, as well as an anticipation of the reduction process. In the non-treated electrode, the reduction of hydrogen peroxide occurs at around – 198 mV, while the same process occurs at – 168 mV at the treated electrode, being closer to 0 V. Thus, the detection of hydrogen peroxide was performed at PB modified pre-treated electrode.

Finally, PB/CB-PLA was employed for the amperometric detection of hydrogen peroxide. Figure 7b shows the amperograms, and respective analytical curve (inset), obtained ($n = 3$) using PB/CB-PLA electrode at 0.0 V (vs. carbon black), after additions of a stock solution of hydrogen peroxide (10.0 mmol L^{-1}) in the electrochemical cell containing 2 mL of supporting electrolyte under magnetic stirring (450 rpm) using a magnetic bar of 9 mm length and diameter of 3 mm. A linear range between 5.0 and 350.0 mol L^{-1} was obtained, following the equation: $-I(\mu A) = 2.40 \times 10^{-8} + 4.18 \times 10^{-8}$ $[H_2O_2]$, with a determination coefficient (R^2) of 0.997. The limits of detection and quantification were calculated according to IUPAC recommendations (described previously), and values of 1.03 µmol L^{-1} and 3.42 µmol L^{-1} were obtained, respectively.

The applicability of PB/CB-PLA was evaluated by the detection of hydrogen peroxide in milk samples. The analysis was performed after simple dilution of the milk with supporting electrolyte (1:1 v/v) followed by fortification with hydrogen peroxide. Aliquots of the sample were then added to the electrochemical cell and an analytical curve was obtained in the sample (Fig. S9) following the equation: $-I(\mu A) = 2.98 \times 10^{-7} + 3.22 \times 10^{-8}$ $[H_2O_2]$, with a determination coefficient (R^2) of 0.993. Recovery values

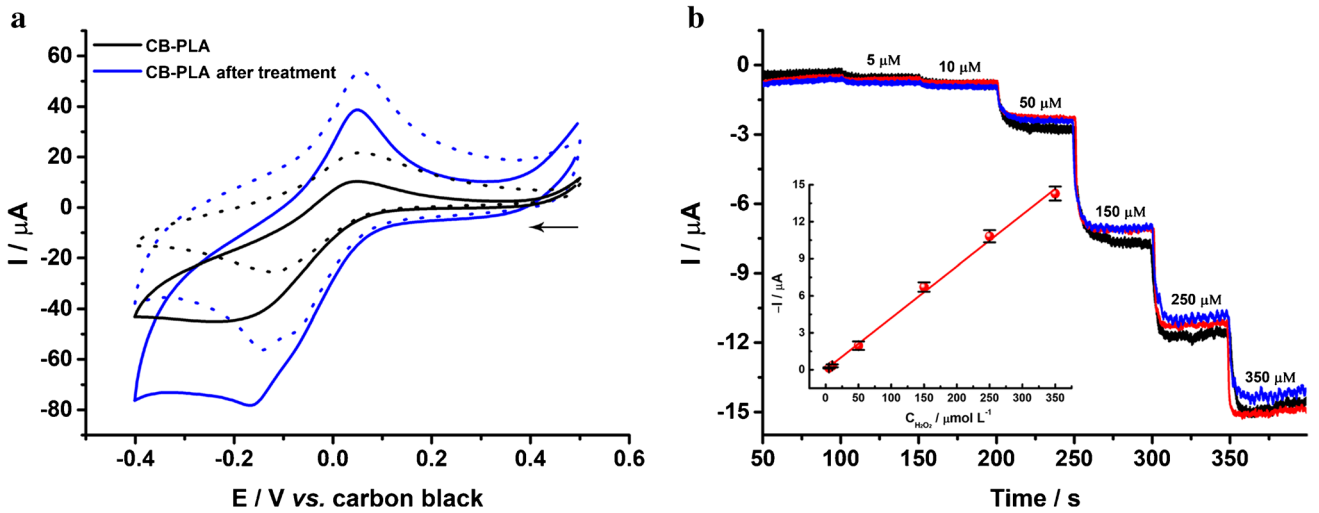

Fig. 7 Cyclic voltammograms recorded for 1.0 mmol L^{-1} hydrogen peroxide using a PB modified CB-PLA 3D-printed electrode (**a**), before (black line) and after (blue line) electrochemical surface treatment. Scan rate: 50 mV s^{-1}; dotted lines: respective blank solution, and **b** amperometric responses ($n = 3$) for increasing concentrations of H_2O_2. Supporting electrolyte: 0.1 mol L^{-1} phosphate buffer solution (pH 7.4) containing 0.1 mol L^{-1} KCl; working potential: 0.0 V (vs. carbon black); inset: respective analytical curve

ranging from 85.2 to 97.1% were obtained (Table S5). The lower recovery values can be attributed to matrix effects from the sample. As reported previously in the literature [49], the high levels of potassium chloride ions contained in milk samples are affecting the ion exchange equilibrium on PB-modified electrode surfaces, which implies in presence of matrix effects when low dilution factors, as employed in this work, are used. However, this problem could be easily circumvented by increasing the sample dilution factor to 10 times [49]. Thus, it is possible to observe the suitability of PB/CB-PLA as a sensor for the non-enzymatic detection of hydrogen peroxide.

Table 1 presents a comparison of the main performance characteristics of PB/CB-PLA against 3D-printed sensors previously reported in the literature. It is possible to observe that the results obtained with the present sensor are in line with those previously described in the literature, demonstrating an excellent performance of the filament made in the laboratory in the construction of a 3D-printed sensor. Furthermore, these results demonstrate that the sensor produced has a great potential for surface modification, giving an excellent perspective for the production of new sensors for the most varied applications.

Thus, the electrodes fabricated using the manufactured CB-PLA filament showed a great performance as an electrochemical sensor for the detection of different compounds, even when applied in complex samples such as milk. It is noteworthy to mention the possibility of manufacturing filaments for 3D printing in adequate amounts according to the need to avoid unnecessary filament storage, circumventing problems such as filament aging, recently reported in the literature [24], which can affect significantly the performance of 3D-printed electrodes. However, the manufacture of conductive composite filaments is poorly explored, and the manufacture of these composites aiming for its use in electroanalysis is even more scarce. Table 2 reports works employed lab-made composite materials or filaments in electroanalysis.

Few composite materials have been proposed for the fabrication of filaments, for 3D printing. Silva et al. [57] employed the obtained composite in the manufacture of a composite graphite paste electrode, and Petroni and collaborators [58] used the fabricated composite in the coating of a 3D-printed surface, obtained from a non-conductive filament after submersion. Thus the advantages of 3D printing are not well explored when compared to works that fabricate composite filaments for direct 3D printing of sensors and devices.

Also, though only a few works report the obtention of conductive filaments for electroanalysis, the fabrication of conductive composite filaments aiming at the manufacture of 3D-printed electronics or other applications can be found in the literature. However, in most cases, the amount of conductive material is low, which can be disadvantageous for the fabrication of electrochemical sensors. Furthermore, in some cases, the fabrication processes involved could lead to non-reproducible sensors, since the incorporation process is not optimized [59–63].

Table 1 Comparison of the analytical characteristics obtained with PB/CB-PLA for the detection of hydrogen peroxide with works reported in the literature

Electrode	Analyte	Linear Range (μmol L^{-1})	LOD (μmol L^{-1})	Ref
GOx-modified 3D-printed biosensor[a]	H_2O_2	50.0–500.0	2.97	[50]
3D pyrolytic carbon microelectrodes	H_2O_2	0.3–8.0	0.16	[51]
PB/G/PLA[b]	H_2O_2	1.0–700.0	0.56	[52]
3DGrE/PB[c]	H_2O_2	1.0–700.0	0.11	[47]
DMF-EC/HRP[d]	H_2O_2	0–100.0 and 150.0–600.0	11.10	[53]
DMF-EC/AuNPs/HRP[e]	H_2O_2	0–100.0 and 150.0–600.0	9.10	[53]
3D e-wells[f]	H_2O_2	1500.0–13,500.0	n.m[h]	[54]
CB/PLA and GR/PLA[g]	H_2O_2	500.0–15,000.0	n.m[h]	[55]
PB/CB-PLA	H_2O_2	5.0–350.0	1.03	This work

[a]3D-printed nanocarbon glucose oxidase-based biosensor

[b]Prussian blue films on additive manufactured electrodes from iron impurities found at the graphene-polylactic acid

[c]3D-printed graphene electrode with Prussian blue

[d]3D-printed graphene-PLA electrode after chemical and electrochemical treatments modified with horseradish peroxidase

[e]3D-printed graphene-PLA electrode after chemical and electrochemical treatments modified with gold nanoparticles plus horseradish peroxidase

[f]3D-printed electrochemical microtitration wells

[g]Carbon black/PLA and graphene/PLA

[h]not mentioned

Table 2 Comparison of the manufacturing characteristics of CB-PLA with lab-made composite materials for electroanalysis of works reported in the literature

Thermoplastic	Conductive material	Composite preparation	Manufacturing time/h	Proposed application	Ref
PLA	Graphene	Dissolution in xylene	6.0 + solvent evaporation	Anode for batteries	[11]
PLA	2D-$MoSe_2$	Dissolution in xylene	6.0 + solvent evaporation	Anode and cathode for WS	[56]
PLA	Graphite	Dissolution in chloroform	96.2	Detection of Pb^{2+} and Cd^{2+}	[57]
ABS	Graphite	Dissolution in acetone	72.2	Detection of PAR	[58]
G-PLA	$Ni(OH)_2$	Dissolution in acetone/chloroform	–	Detection of glucose	[17]
PLA	NG	Dissolution in xylene	6.0 + solvent evaporation	Detection of Pb^{2+} and Cd^{2+}	[18]
PLA	Graphite	Dissolution in acetone/chloroform	15.5	Detection of UA, DA, and SARS-CoV-2	[13]
PLA	Carbon black	Dissolution in acetone/chloroform	15.2	Detection of CA, HQ, and H_2O_2	This work

DA dopamine, *NG* nanographite, *PAR* paracetamol, *UA* uric acid, *WS* water splitting

Nonetheless, it is noteworthy to mention that the increased amount of conductive material in the proposed filament, though provides improved electrochemical performance, also show some drawbacks. In comparison to the commercial Proto-pasta, the proposed filament is less flexible, requiring more careful handling. A comparison between the flexibility of CB-PLA and Proto-pasta filaments is presented in the supplementary material. Figure S10 shows the images demonstrating the maximum mechanical stress allowed for CB-PLA (Fig. S10-a) and Proto-pasta (Fig. S10-c), and the respective damage caused after more stress is applied (Fig. S10-b and S10-d). As can be observed, Proto-pasta filaments withstand greater stress than CB-PLA. Due to the increased rigidity of CB-PLA, when undergoing more stress, the filament breaks (Fig. S10-b), which is not observed for Proto-pasta (Fig. S10-d). However, though Proto-pasta is not breaking after more stress, the filament is significantly damaged, being bent after the over stress is applied as can be observed in the inset of Fig. S10-d. The lower flexibility of CB-PLA is not significantly impairing the printing process. A simple reduction in print speed (reducing the printing time between 10 and 20%) and adjusting printability, could provide the obtention of electrodes with high printing quality, comparable to the obtained with Proto-pasta filaments.

In addition to this, temperature and humidity can influence the quality of the obtained filaments and sensors. In fact, on warmer days, the extrusion of the filaments is highly impaired, occasioning the obtention of thin filaments due to the melting and prolonged cooling process. However, this can be circumvented by the use of an air-conditioned room, at mild temperatures, or the use of a cooling system with fans. Additionally, the performance of the electrodes obtained from the lab-made filaments is affected by humidity, and a loss in the electrochemical response is observed. Nonetheless, this issue is observed for most of the 3D-printed sensors, obtained from PLA-based filaments, including commercial ones [24]. Adequate storage of the filaments and electrodes, avoiding humidity, dust or contaminations is recommended, this will increase the lifetime of the 3D-printed electrodes. The stability of electrodes was performed with the proposed CB-PLA filament, stored adequately in a dry place inside a sealed plastic bag for 6 months, and the results were compared to the voltammogram obtained using the same electrode as printed. For this, both electrodes were carefully polished to renew the surface, and a new surface treatment using 0.5 mol L^{-1} NaOH solution was performed previous to the measurements. Fig. S11 shows the voltammograms for the readily printed electrode (black line), and for the electrode after 6 months stored (red line), recorded using a using 1.0 mmol L^{-1} ferrocene methanol solution prepared in 0.1 mol L^{-1} KCl. The anodic peak current decreased from 50.5 to 47.6 µA, corresponding to a decrease of 5.7%, while the cathodic peak current decreased from 40.0 to 37.5 µA (3.7% decrease). Considering these results, it can be seen that after 6 months, the electrode is still stable and can be employed for electrochemical analysis.

Conclusions

The present work reports the lab-made manufacturing of a composite filament based on carbon black and polylactic acid, which can supply laboratories and research centers in a simple, low-cost, and easy-to-produce way. The proposed filament showed improved electrochemical characteristics as an electrochemical sensor when compared to the commercially available CB-based filament due to its higher and optimized CB loading. Thus, it was possible to obtain conductive filaments with 28.5% wt. of CB, which represents an increase of approximately 7% in comparison to the commercial filament. This increase, in terms of total conductive material, represents 30% more CB used, which led to superior electrochemical performance. Though

the CB-PLA 3D printed electrodes obtained with the proposed filament presented an electrochemical response without surface activation procedures, we showed that the saponification reaction of the PLA from the surface of the electrode after electrochemical pretreatment improved significantly the performance of the electrodes, providing enhanced electrochemical processes, with higher peak current responses and a decrease in the peak-to-peak separation.

The improved CB-PLA electrodes obtained from the lab-made filaments showed adequate performance in the detection of catechol, hydroquinone, and hydrogen peroxide, allowing the detection of hydrogen peroxide even in complex samples such as milk and water samples. In addition, the suitability of the obtained sensors as a platform for the anchoring of species was also demonstrated by the electrode modification with Prussian blue particles. In this sense, the different applications show that additive manufacturing of improved electrochemical sensors can be performed by the simple and low-cost fabrication, in a decentralized way, of conductive filaments. The filaments can be produced according to the demand, and are versatile to be manufactured, enabling different compositions and materials, eliminating the need to purchase or, in some cases, import the commercial filaments which have a fixed and often unknown composition. In addition, the possibility of manufacturing filaments in the laboratory circumvents problems such as filament aging, since they can be produced in smaller amounts, according to need, avoiding unnecessary filament storage.

Supplementary Information The online version contains supplementary material available at https://doi.org/10.1007/s00604-022-05511-2.

Acknowledgements The authors are grateful to the Brazilian agencies FAPESP (2017/21097-3 and 2022/06145-0), CAPES (001), CAPES (88887.636021/2021-00 and 88887.510880/2020-00), and CNPq (303338/2019-9) for the financial support. We also acknowledge the Institute of Physics (INFIS) of the Federal University of Uberlandia for Raman (Horiba LabRAM HR Evolution Raman) spectroscopic measurements supported by the grant "Pró-Equipamentos" from the Brazilian agency CAPES and by FINEP.

Declarations

Conflict of interest The authors declare no conflict of interest.

References

1. Cardoso RM, Kalinke C, Rocha RG, dos Santos PL, Rocha DP, Oliveira PR, Janegitz BC, Bonacin JA, Richter EM, Munoz RAA (2020) Additive-manufactured (3D-printed) electrochemical sensors: a critical review. Anal Chim Acta 1118:73–91. https://doi.org/10.1016/j.aca.2020.03.028
2. Hamzah HH, Shafiee SA, Abdalla A, Patel BA (2018) 3D printable conductive materials for the fabrication of electrochemical sensors: a mini review. Electrochem commun 96:27–31. https://doi.org/10.1016/j.elecom.2018.09.006
3. Stefano JS, Kalinke C, Da Rocha RG, Rocha DP, Da Silva VAOP, Bonacin JA, Angnes L, Richter EM, Janegitz BC, Muñoz RAA (2022) Electrochemical (Bio)sensors enabled by fused deposition modeling-based 3D Printing: a guide to selecting designs, printing parameters, and post-treatment protocols. Anal Chem 94:6417–6429. https://doi.org/10.1021/acs.analchem.1c05523
4. Silva LRG, Gevaerd A, Marcolino-Junior LH, Bergamini MF, Silva TA, Janegitz BC (2022) 3D-printed electrochemical devices for sensing and biosensing of biomarkers. In: Advances in Bioelectrochemistry Volume 2. Springer International Publishing, pp 121–136
5. Manzanares-Palenzuela CL, Hermanova S, Sofer Z, Pumera M (2019) Proteinase-sculptured 3D-printed graphene/polylactic acid electrodes as potential biosensing platforms: towards enzymatic modeling of 3D-printed structures. Nanoscale 11:12124–12131. https://doi.org/10.1039/C9NR02754H
6. Silva VAOP, Fernandes-Junior WS, Rocha DP, Stefano JS, Munoz RAA, Bonacin JA, Janegitz BC (2020) 3D-printed reduced graphene oxide/polylactic acid electrodes: a new prototyped platform for sensing and biosensing applications. Biosens Bioelectron 170:112684. https://doi.org/10.1016/j.bios.2020.112684
7. Zafir Mohamad Nasir M, Novotný F, Alduhaish O, Pumera M (2020) 3D-printed electrodes for the detection of mycotoxins in food. Electrochem commun 115:106735. https://doi.org/10.1016/j.elecom.2020.106735
8. Richter EM, Rocha DP, Cardoso RM, Keefe EM, Foster CW, Munoz RAA, Banks CE (2019) Complete additively manufactured (3D-printed) electrochemical sensing platform. Anal Chem 91:12844–12851. https://doi.org/10.1021/acs.analchem.9b02573
9. Muñoz J, Pumera M (2020) Accounts in 3D-printed electrochemical sensors: Towards monitoring of environmental pollutants. ChemElectroChem 7:3404–3413. https://doi.org/10.1002/celc.202000601
10. Foster CW, Down MP, Zhang Y, Ji X, Rowley-Neale SJ, Smith GC, Kelly PJ, Banks CE (2017) 3D Printed graphene based energy storage devices. Sci Rep 7:42233. https://doi.org/10.1038/srep42233
11. Foster CW, Zou G, Jiang Y, Down MP, Liauw CM, Garcia-Miranda Ferrari A, Ji X, Smith GC, Kelly PJ, Banks CE (2019) Next-Generation Additive Manufacturing: Tailorable Graphene/Polylactic(acid) Filaments allow the fabrication of 3D printable porous anodes for utilisation within lithium-ion batteries. Batter Supercaps 2:448–453. https://doi.org/10.1002/batt.201800148
12. Elbardisy HM, Richter EM, Crapnell RD, Down MP, Gough PG, Belal TS, Talaat W, Daabees HG, Banks CE (2020) Versatile additively manufactured (3D printed) wall-jet flow cell for high performance liquid chromatography-amperometric analysis: application to the detection and quantification of new psychoactive substances (NBOMes). Anal Methods 12:2152–2165. https://doi.org/10.1039/d0ay00500b
13. Stefano JS, Guterres e Silva LR, Rocha RG, Brazaca LC, Richter EM, Abarza Muñoz RA, Janegitz BC (2021) New conductive filament ready-to-use for 3D-printing electrochemical (bio)sensors: towards the detection of SARS-CoV-2. Anal Chim Acta 1191:339372. https://doi.org/10.1016/J.ACA.2021.339372
14. Kalkal A, Kumar S, Kumar P, Pradhan R, Willander M, Packirisamy G, Kumar S, Malhotra BD (2021) Recent advances in 3D printing technologies for wearable (bio)sensors. Addit Manuf 46:102088. https://doi.org/10.1016/j.addma.2021.102088
15. Contreras-Naranjo JE, Perez-Gonzalez VH, Mata-Gómez MA, Aguilar O (2021) 3D-printed hybrid-carbon-based electrodes for electroanalytical sensing applications. Electrochem commun 130:107098. https://doi.org/10.1016/j.elecom.2021.107098
16. O'Neil GD (2020) Toward single-step production of functional electrochemical devices using 3D printing: Progress, challenges, and opportunities. Curr Opin Electrochem 20:60–65
17. Rocha RG, Cardoso RM, Zambiazi PJ, Castro SVF, Ferraz TVB, de Aparecido GO, Bonacin JA, Munoz RAA, Richter EM (2020) Production of 3D-printed disposable electrochemical sensors

for glucose detection using a conductive filament modified with nickel microparticles. Anal Chim Acta 1132:1–9. https://doi.org/10.1016/j.aca.2020.07.028
18. Foster CW, Elbardisy HM, Down MP, Keefe EM, Smith GC, Banks CE (2020) Additively manufactured graphitic electrochemical sensing platforms. Chem Eng J 381:122343. https://doi.org/10.1016/j.cej.2019.122343
19. Silva TA, Moraes FC, Janegitz BC, Fatibello-Filho O (2017) Electrochemical biosensors based on nanostructured carbon black: a review. J Nanomater 2017:1–14. https://doi.org/10.1155/2017/4571614
20. (2018) Conductive PLA Proto-Pasta Safety Datasheet. https://filament2print.com/gb/index.php?controller=attachment&id_attachment=94. Accessed 25 Jun 2022
21. Cardoso RM, Mendonça DMH, Silva WP, Silva MNT, Nossol E, da Silva RAB, Richter EM, Muñoz RAA (2018) 3D printing for electroanalysis: from multiuse electrochemical cells to sensors. Anal Chim Acta 1033:49–57. https://doi.org/10.1016/j.aca.2018.06.021
22. da Silva VAOP, Tartare VAP, Kalinke C, de Oliveira PR, de Souza DC, Bonacin JA, Janegitz BC (2020) Lab-made 3D-printed contact angle measurement adjustable holder. Quim Nova 43:1312–1319
23. Jiang Y, Zhang X, Shan C, Hua S, Zhang Q, Bai X, Dan L, Niu L (2011) Functionalization of graphene with electrodeposited Prussian blue towards amperometric sensing application. Talanta 85:76–81. https://doi.org/10.1016/j.talanta.2011.03.028
24. Kalinke C, de Oliveira PR, Neumsteir NV, Henriques BF, de Oliveira Aparecido G, Loureiro HC, Janegitz BC, Bonacin JA (2022) Influence of filament aging and conductive additive in 3D printed sensors. Anal Chim Acta 1191:33228. https://doi.org/10.1016/j.aca.2021.339228
25. Katseli V, Thomaidis N, Economou A, Kokkinos C (2020) Miniature 3D-printed integrated electrochemical cell for trace voltammetric Hg(II) determination. Sensors Actuators, B Chem 308:127715. https://doi.org/10.1016/j.snb.2020.127715
26. Vaněčková E, Bouša M, Nováková Lachmanová Š, Rathouský J, Gál M, Sebechlebská T, Kolivoška V (2020) 3D printed polylactic acid/carbon black electrodes with nearly ideal electrochemical behaviour. J Electroanal Chem 857:113745. https://doi.org/10.1016/j.jelechem.2019.113745
27. Cardoso RM, Rocha DP, Rocha RG, Stefano JS, Silva RAB, Richter EM, Muñoz RAA (2020) 3D-printing pen versus desktop 3D-printers: Fabrication of carbon black/polylactic acid electrodes for single-drop detection of 2,4,6-trinitrotoluene. Anal Chim Acta 1132:10–19. https://doi.org/10.1016/j.aca.2020.07.034
28. Bokobza L, Bruneel J-L, Couzi M (2015) Raman spectra of carbon-based materials (from graphite to carbon black) and of some silicone composites. C J Carbon Res 1:77–94. https://doi.org/10.3390/c1010077
29. Ferrari AGM, Foster CW, Kelly PJ, Brownson DAC, Banks CE (2018) Determination of the electrochemical area of screen-printed electrochemical sensing platforms. Biosensors 8:1–10. https://doi.org/10.3390/bios8020053
30. Amatore C, Da Mota N, Sella C, Thouin L (2007) Theory and experiments of transport at channel microband electrodes under laminar flows. 1. Steady-state regimes at a single electrode. Anal Chem 79:8502–8510. https://doi.org/10.1021/ac070971y
31. Randviir EP, Banks CE (2013) Electrochemical impedance spectroscopy: an overview of bioanalytical applications. Anal Methods 5:1098. https://doi.org/10.1039/c3ay26476a
32. Ahmed J, Faisal M, Jalalah M, Alsaiari M, Alsareii SA, Harraz FA (2021) An efficient amperometric catechol sensor based on novel polypyrrole-carbon black doped α-Fe2O3 nanocomposite. Colloids Surfaces A Physicochem Eng Asp 619:126469. https://doi.org/10.1016/j.colsurfa.2021.126469
33. Raymundo-Pereira PA, Campos AM, Mendonça CD, Calegaro ML, Machado SAS, Oliveira ON (2017) Printex 6L carbon nanoballs used in electrochemical sensors for simultaneous detection of emerging pollutants hydroquinone and paracetamol. Sensors Actuators B Chem 252:165–174. https://doi.org/10.1016/j.snb.2017.05.121
34. Ören Varol T, Hakli O, Anik U (2021) Graphene oxide-porphyrin composite nanostructure included electrochemical sensor for catechol detection. New J Chem 45:1734–1742. https://doi.org/10.1039/d0nj05475e
35. Peng Y, Tang ZR, Dong YP, Che G, Xin ZF (2018) Electrochemical detection of hydroquinone based on MoS2/reduced graphene oxide nanocomposites. J Electroanal Chem 816:38–44. https://doi.org/10.1016/j.jelechem.2018.03.034
36. O'Neil GD, Ahmed S, Halloran K, Janusz JN, Rodríguez A, Terrero Rodríguez IM (2019) Single-step fabrication of electrochemical flow cells utilizing multi-material 3D printing. Electrochem commun 99:56–60. https://doi.org/10.1016/j.elecom.2018.12.006
37. Kapan B, Kurbanoglu S, Esenturk EN, Soylemez S, Toppare L (2021) Electrochemical catechol biosensor based on β-cyclodextrin capped gold nanoparticles and inhibition effect of ibuprofen. Process Biochem 108:80–89. https://doi.org/10.1016/j.procbio.2021.06.004
38. Indrajith Naik E, Sunil Kumar Naik TS, Pradeepa E, Singh S, Naik HSB (2022) Design and fabrication of an innovative electrochemical sensor based on Mg-doped ZnO nanoparticles for the detection of toxic catechol. Mater Chem Phys 281. https://doi.org/10.1016/j.matchemphys.2022.125860
39. Liu T, Xie Y, Shi L, Liu Y, Chu Z, Jin W (2021) 3D Prussian blue/Pt decorated carbon nanofibers based screen-printed microchips for the ultrasensitive hydroquinone biosensing. Chinese J Chem Eng 37:105–113. https://doi.org/10.1016/j.cjche.2021.02.017
40. Maciel CC, de Lima LF, Ferreira AL, de Araujo WR, Ferreira M (2022) Development of a flexible and disposable electrochemical sensor based on poly (butylene adipate-co-terephthalate) and graphite for hydroquinone sensing. Sens Actuators Reports 4:100091. https://doi.org/10.1016/j.snr.2022.100091
41. Park J, Kim J, Min A, Choi MY (2022) Fabrication of nonenzymatic electrochemical sensor based on Zn@ZnO core-shell structures obtained via pulsed laser ablation for selective determination of hydroquinone. Environ Res 204:112340. https://doi.org/10.1016/j.envres.2021.112340
42. Ming SS, Gowthaman NSK, Lim HN, Arul P, Narayanamoorthi E, Ibrahim I, Jaafar H, John SA (2021) Aluminium MOF fabricated electrochemical sensor for the ultra-sensitive detection of hydroquinone in water samples. J Electroanal Chem 883:115067. https://doi.org/10.1016/j.jelechem.2021.115067
43. Muslu E, Eren E, Oksuz AU (2022) Prussian blue-based flexible thin film nanoarchitectonics for non-enzymatic electrochemical glucose sensor. J Inorg Organomet Polym Mater 1:1–10. https://doi.org/10.1007/s10904-022-02290-4
44. Liu X, Zhang X, Zheng J (2021) One-pot fabrication of AuNPs-Prussian blue-Graphene oxide hybrid nanomaterials for non-enzymatic hydrogen peroxide electrochemical detection. Microchem J 160:105595. https://doi.org/10.1016/j.microc.2020.105595
45. Rojas D, Della Pelle F, Del Carlo M, D'Angelo M, Dominguez-Benot R, Cimini A, Escarpa A, Compagnone D (2018) Electrodeposited Prussian Blue on carbon black modified disposable electrodes for direct enzyme-free H2O2 sensing in a Parkinson's disease in vitro model. Sensors Actuators, B Chem 275:402–408. https://doi.org/10.1016/j.snb.2018.08.040
46. Husmann S, Orth ES, Zarbin AJG (2019) A multi-technique approach towards the mechanistic investigation of the electrodeposition of Prussian blue over carbon nanotubes film. Electrochim Acta 312:380–391. https://doi.org/10.1016/j.electacta.2019.04.141

47. Katic V, Dos Santos PL, Dos Santos MF, Pires BM, Loureiro HC, Lima AP, Queiroz JCM, Landers R, Muñoz RAA, Bonacin JA (2019) 3D Printed graphene electrodes modified with Prussian blue: emerging electrochemical sensing platform for peroxide detection. ACS Appl Mater Interfaces 11:35068–35078. https://doi.org/10.1021/acsami.9b09305
48. Karyakin AA, Karyakina EE, Gorton L (1999) On the mechanism of H2O2 reduction at Prussian Blue modified electrodes. Electrochem commun 1:78–82. https://doi.org/10.1016/S1388-2481(99)00010-7
49. Silva RAB, Montes RHO, Richter EM, Munoz RAA (2012) Rapid and selective determination of hydrogen peroxide residues in milk by batch injection analysis with amperometric detection. Food Chem 133:200–204. https://doi.org/10.1016/j.foodchem.2012.01.003
50. Wang L, Pumera M (2021) Covalently modified enzymatic 3D-printed bioelectrode. Microchim Acta 188:1–8. https://doi.org/10.1007/s00604-021-05006-6
51. Esmail Tehrani S, Quang Nguyen L, Garelli G, Jensen BM, Ruzgas T, Emnéus J, Sylvest Keller S (2021) Hydrogen peroxide detection using prussian blue-modified 3D pyrolytic carbon microelectrodes. Electroanalysis 33:2516–2528. https://doi.org/10.1002/elan.202100387
52. Rocha RG, Stefano JS, Cardoso RM, Zambiazi PJ, Bonacin JA, Richter EM, Munoz RAA (2020) Electrochemical synthesis of Prussian blue from iron impurities in 3D-printed graphene electrodes: Amperometric sensing platform for hydrogen peroxide. Talanta 219:121289. https://doi.org/10.1016/j.talanta.2020.121289
53. López Marzo AM, Mayorga-Martinez CC, Pumera M (2020) 3D-printed graphene direct electron transfer enzyme biosensors. Biosens Bioelectron 151:11980. https://doi.org/10.1016/j.bios.2019.111980
54. Katseli V, Angelopoulou M, Kokkinos C (2021) 3D printed bioelectronic microwells. Adv Funct Mater 31:102459. https://doi.org/10.1002/adfm.202102459
55. Abdalla A, Perez F, Cañadas AT, Ray S, Patel BA (2021) How normalisation factors influence the interpretations of 3D-printed sensors for electroanalysis. J Electroanal Chem 881:114937. https://doi.org/10.1016/j.jelechem.2020.114937
56. Hughes JP, Dos Santos L, Down MP, Foster CW, Bonacin JA, Keefe EM, Rowley-Neale SJ, Banks CE (2020) Single step additive manufacturing (3D printing) of electrocatalytic anodes and cathodes for efficient water splitting †. Sustain Energy Fuels 4:302. https://doi.org/10.1039/c9se00679f
57. Silva AL, Corrêa MM, De Oliveira GC, Michel RC, Semaan FS, Ponzio EA (2018) Development and application of a routine robust graphite/poly(lactic acid) composite electrode for the fast simultaneous determination of Pb2+ and Cd2+ in jewelry by square wave anodic stripping voltammetry. New J Chem 42:19537–19547. https://doi.org/10.1039/c8nj03501f
58. Petroni JM, Neves MM, de Moraes NC, Bezerra da Silva RA, Ferreira VS, Lucca BG (2021) Development of highly sensitive electrochemical sensor using new graphite/acrylonitrile butadiene styrene conductive composite and 3D printing-based alternative fabrication protocol. Anal Chim Acta 1167:338566. https://doi.org/10.1016/j.aca.2021.338566
59. Cruz MA, Ye S, Kim MJ, Reyes C, Yang F, Flowers PF, Wiley BJ (2018) Multigram synthesis of Cu-Ag core-shell nanowires enables the production of a highly conductive polymer filament for 3D printing electronics. Part Part Syst Charact 35:1700385. https://doi.org/10.1002/ppsc.201700385
60. Wei X, Li D, Jiang W, Gu Z, Wang X, Zhang Z, Sun Z (2015) 3D Printable Graphene Composite. Sci Rep 5:11181. https://doi.org/10.1038/srep11181
61. Kwok SW, Goh KHH, Tan ZD, Tan STM, Tjiu WW, Soh JY, Ng ZJG, Chan YZ, Hui HK, Goh KEJ (2017) Electrically conductive filament for 3D-printed circuits and sensors. Appl Mater Today 9:167–175. https://doi.org/10.1016/j.apmt.2017.07.001
62. Nabipour M, Akhoundi B (2021) An experimental study of FDM parameters effects on tensile strength, density, and production time of ABS/Cu composites. J Elastomers Plast 53:146–164. https://doi.org/10.1177/0095244320916838
63. Leigh SJ, Bradley RJ, Purssell CP, Billson DR, Hutchins DA (2012) A simple, low-cost conductive composite material for 3D printing of electronic sensors. PLoS One 7:e9365. https://doi.org/10.1371/journal.pone.0049365
64. Ambrosi A, Pumera M (2016) 3D-printing technologies for electrochemical applications. Chem Soc Rev 45:2740–2755. https://doi.org/10.1039/c5cs00714c
65. Ngo TD, Kashani A, Imbalzano G, Nguyen KTQ, Hui D (2018) Additive manufacturing (3D printing): a review of materials, methods, applications and challenges. Compos Part B Eng 143:172–196. https://doi.org/10.1016/J.COMPOSITESB.2018.02.012
66. Oladapo BI, Ismail SO, Afolalu TD, Olawade DB, Zahedi M (2021) Review on 3D printing: fight against COVID-19. Mater Chem Phys 258:123943. https://doi.org/10.1016/J.MATCHEMPHYS.2020.123943
67. Longhitano GA, Nunes GB, Candido G, da Silva JVL (2021) The role of 3D printing during COVID-19 pandemic: a review. Prog Addit Manuf 6:19–37. https://doi.org/10.1007/S40964-020-00159-X
68. Carrasco-Correa EJ, Simó-Alfonso EF, Herrero-Martínez JM, Miró M (2021) The emerging role of 3D printing in the fabrication of detection systems. TrAC - Trends Anal Chem 136:116177
69. Abdalla A, Patel BA (2020) 3D-printed electrochemical sensors: a new horizon for measurement of biomolecules. Curr Opin Electrochem 20:78–81. https://doi.org/10.1016/j.coelec.2020.04.009
70. Browne MP, Novotný F, Sofer Z, Pumera M (2018) 3D printed graphene electrodes' electrochemical activation. ACS Appl Mater Interfaces 10:40294–40301. https://doi.org/10.1021/acsami.8b14701
71. Manzanares Palenzuela CL, Novotný F, Krupička P, Sofer Z, Pumera M (2018) 3D-printed graphene/polylactic acid electrodes promise high sensitivity in electroanalysis. Anal Chem 90:5753–5757. https://doi.org/10.1021/acs.analchem.8b00083
72. Pereira JFS, Rocha RG, Castro SVF, João AF, Borges PHS, Rocha DP, de Siervo A, Richter EM, Nossol E, Gelamo RG, Muñoz RAA (2021) Reactive oxygen plasma treatment of 3D-printed carbon electrodes towards high-performance electrochemical sensors. Sensors Actuators B Chem 347:130651. https://doi.org/10.1016/j.snb.2021.130651
73. Rocha DP, Ataide VN, de Siervo A, Gonçalves JM, Muñoz RAA, Paixão TRLC, Angnes L (2021) Reagentless and subminute laser-scribing treatment to produce enhanced disposable electrochemical sensors via additive manufacture. Chem Eng J 425:130594. https://doi.org/10.1016/j.cej.2021.130594